

Laser and decay spectroscopy of the short-lived isotope ^{214}Fr in the vicinity of the $N = 126$ shell closure

G. J. Farooq-Smith,^{1,2,*} T. E. Cocolios,^{1,2} J. Billowes,¹ M. L. Bissell,^{1,2} I. Budinčević,² T. Day Goodacre,^{1,3} R. P. de Groot,² V. N. Fedosseev,³ K. T. Flanagan,¹ S. Franchoo,⁴ R. F. Garcia Ruiz,^{1,2} H. Heylen,² R. Li,^{4,†} K. M. Lynch,^{2,5} B. A. Marsh,³ G. Neyens,² R. E. Rossel,^{3,6} S. Rothe,^{1,3} H. H. Stroke,⁷ K. D. A. Wendt,⁶ S. G. Wilkins,¹ and X. F. Yang²

¹*School of Physics and Astronomy, The University of Manchester, Manchester M13 9PL, United Kingdom*

²*KU Leuven, Instituut voor Kern- en Stralingsfysica, B-3001 Leuven, Belgium*

³*EN Department, CERN, CH-1211 Geneva 23, Switzerland*

⁴*Institut de Physique Nucléaire d'Orsay, F-91406 Orsay, France*

⁵*ISOLDE, PH Department, CERN, CH-1211 Geneva 23, Switzerland*

⁶*Institut für Physik, Johannes Gutenberg-Universität, D-55128 Mainz, Germany*

⁷*Department of Physics, New York University, New York, New York 10003, USA*

(Received 10 August 2016; published 4 November 2016; publisher error corrected 17 November 2016)

Combined decay and laser spectroscopy measurements of the isotope ^{214}Fr are reported, using the collinear resonance ionization spectroscopy (CRIS) technique at the ISOLDE facility at CERN. For the $I^\pi = (1^-)$ spin assignment, the g -factor value of $g(^{214}\text{Fr}) = +0.241(16)$ corresponds to a relatively pure $(\pi 1h_{9/2} \otimes \nu 2g_{9/2})$ ground-state configuration. An alternative interpretation with $g(^{214}\text{Fr}) = +0.144(10)$, for a (2^-) spin assignment suggests a greater contribution of configuration mixing with the $\nu 1i_{11/2}$ orbital. As the $N = 126$ shell closure is passed, a kink is observed at the $\delta\langle r^2 \rangle^{213,214}$ value, which is analogous to the behavior observed in the neighboring isotopic chains.

DOI: [10.1103/PhysRevC.94.054305](https://doi.org/10.1103/PhysRevC.94.054305)

I. INTRODUCTION

As one of the first elements studied at the isotope separator online device (ISOLDE) facility at CERN [1], francium has played an important role in explaining the variety of nuclear behavior that exists around the $Z = 82$ and $N = 126$ magic shell closures. High-profile studies have already documented the phenomena of shape coexistence and octupole deformations in isotopes located in the neutron-deficient and -rich regions, respectively [2,3]. However, for the case of $^{214}\text{Fr}_{127}$, which resides between these two regions next to the $N = 126$ shell closure, little information is known. In this paper we focus on the charge radii in the trans-lead region and in particular, the characteristic increase in the gradient that is observed at a shell closure crossing. This is often referred to as a “kink” [4] and has already been seen at $N = 126$ in the neighboring isotopes from thallium to radium [5–12].

The interpretation of the kink at $N = 126$ remains a challenge for nuclear models. Many groups have investigated this region with mean-field calculations [13–17] but no general consensus exists on how to reproduce the correct magnitudes. Until now, limited experimental input has been available regarding the gradient of the kink at this particular shell

closure. Although data for the trans-lead region is available from $N = 132$ onwards, little is known for $N = 127$ – 131 due to the short lifetime of the isotopes immediately after the $N = 126$ shell closure. Only four $N = 127$ isotones have been studied: ^{81}Tl [5], ^{82}Pb [6], ^{83}Bi [7], and ^{84}Po [18]. With five protons located in the $\pi 1h_{9/2}$ orbital, ^{214}Fr offers an additional test of the robustness of the $Z = 82$ shell closure.

The collinear resonance ionization spectroscopy (CRIS) setup at CERN-ISOLDE has recently explored isotopes across the francium chain [11,19–22]. In particular, new developments at the decay spectroscopy station (DSS) [23] have allowed combined decay and laser spectroscopy techniques to be performed. A recent example of this includes the identification of ground and isomeric states in ^{202}Fr , ^{204}Fr , and ^{206}Fr [20,22], from overlapping hyperfine structures. In this article, we report the first measurements of ^{214}Fr at the CRIS beam line. With a half-life of only 5.0(2) ms [24], ^{214}Fr represents the shortest-lived isotope to have been measured online with laser spectroscopy. The change in the mean-square charge-radii and the gyromagnetic factor will be presented, alongside a discussion on recent mean-field calculations performed in the area. Based on these considerations, the implications on the behavior exhibited past the $N = 126$ shell closure will be discussed.

II. EXPERIMENTAL SETUP

The ^{214}Fr ion beam was produced at the ISOLDE facility [25] via spallation reactions, by impinging 1.4 GeV protons from the proton-synchrotron booster (PSB) onto a thick UC_x target [26]. The PSB duty cycle delivered proton pulses separated by integral multiples of 1.2 s, resulting in release profiles that could be defined empirically [27]. The short

*gregoryjames.farooqsmith@kuleuven.be

†Present address: TRIUMF, Vancouver, British Columbia V6T 2A3, Canada.

Published by the American Physical Society under the terms of the [Creative Commons Attribution 3.0 License](https://creativecommons.org/licenses/by/3.0/). Further distribution of this work must maintain attribution to the author(s) and the published article's title, journal citation, and DOI.

half-life of ^{214}Fr meant that the release profile was primarily dominated by the decay losses. This increased the importance of operating the experimental setup at a fast duty cycle comparable to the half-life, in order to minimize these losses.

The resulting reaction products were surface-ionized in a high temperature (~ 2200 K) tantalum hot cavity ion source and extracted at 40 keV. The isotopes of interest were mass separated by the high resolution mass separator (HRS) [25]. Cooling and bunching of the ions was performed with the use of the ISCOOL radio-frequency gas-filled linear Paul trap [28,29]. The release time for these bunches was synchronized with the duty cycle of the laser system. In order to limit the ^{214}Fr decay losses from within the trap, a 200 Hz repetition rate was used. After reaccelerating to 40 keV, the ion bunches were electrostatically deflected into the CRIS beam line [20,30,31], where they were first neutralized through a charge exchange cell (CEC) filled with potassium vapor (445–455 K) with a neutralization efficiency of $\sim 50\%$. Any remaining nonneutralized ions were deflected out of the atomic beam in the differential pumping region situated just after the CEC.

The neutralized atomic bunches then entered an ultra high vacuum (UHV) interaction region (kept at a pressure of 9×10^{-9} mbar), where they were collinearly overlapped with laser light both spatially and temporally. The ionization scheme consisted of two steps: a 422.7-nm step to excite the $7s^2S_{1/2} \rightarrow 8p^2P_{3/2}$ transition at $23\,658.306\text{ cm}^{-1}$, and a nonresonant 1064-nm step, which was subsequently used to ionize the atoms. The 422.7-nm laser light was produced by frequency-doubling light from a 10 kHz Ti:Sa narrowband (1 GHz) laser provided by the resonance ionization laser source (RILIS) laser laboratory [32,33], in which the laser frequency could be stepped by using a data acquisition routine [34]. It was transported to the CRIS beam line using a 35-m long multimode optical fiber. The 1064-nm light was produced with a Litron LPY-601 Nd:YAG system (consisting of two lasers running at 100 Hz each) that could operate at 200 Hz, situated next to the CRIS beam line. By opening the beam gate 10 ms after proton impact with the target and setting its temporal width to several ^{214}Fr half-lives, the amount of ^{214}Fr available for study was maximized. This also limited the isobaric contamination present (mainly ^{214}Ra), which was constantly released from the target. The low pressure maintained within the interaction region minimized the background due to nonresonant ionization with gas molecules. After the resonant excitation and reionization processes, the ions were deflected onto a biased copper plate (held at -270 V), where ejected secondary electrons were guided onto a micro-channel plate (MCP) detector. Separate α -decay spectroscopy could also be performed by implanting the ions into carbon foils on a rotatable wheel. Emitted α particles could be detected within the DSS [20,23], located at the end of the CRIS beam line.

III. RESULTS

A. Laser spectroscopy of ^{214}Fr

The magnetic dipole moment was extracted from the hyperfine structure shown in Fig. 1 by means of a χ^2 -minimization fitting routine [4]. The center of gravity of the

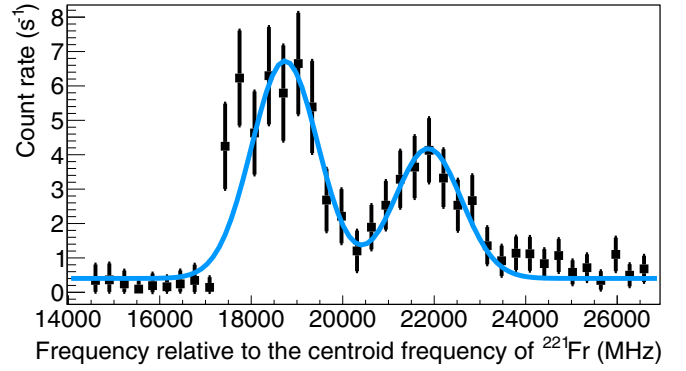


FIG. 1. Collinear resonance ionization spectroscopy of ^{214}Fr . Each data point represents an average of 72 s of data recording.

hyperfine spectrum of ^{214}Fr was compared to the reference isotope, ^{221}Fr , for extraction of the isotope shift. All other measured observables were determined relative to ^{210}Fr , using: $A_{\text{ref}}(7s^2S_{1/2}) = +7195.1(4)$ MHz [35], $I^\pi = 6^+$ [36], and $\mu_{\text{ref}} = +4.38(5) \mu_N$ [37]. The changes in the mean-square charge radii were extracted by using the equation

$$\delta v^{AA'} = M_{422} \frac{A' - A}{AA'} + F_{422} \delta \langle r^2 \rangle^{AA'}, \quad (1)$$

where A and A' are assigned to the reference and measured isotopes, respectively. The parameters $M_{422} = +750(330)$ GHz.amu and $F_{422} = -20.67(21)$ GHz/fm 2 represent the atomic factors and contain all the optical dependence for the 422.7-nm transition [20]. The hyperfine anomaly for francium has been measured as $<1\%$ [40,41], which was beyond the resolution of the technique used in this work. The data were analyzed with a constant ratio of $A(7s^2S_{1/2})/A(7p^2P_{3/2}) = +0.0036$ and the $B(7p^2P_{3/2})$ hyperfine parameter was set to zero [30]. The 1.5-GHz line width of the 422.7-nm RILIS Ti:Sa laser produced pure Gaussian line shapes. Only the lower-state splitting could be resolved, preventing the extraction of the nuclear spin and quadrupole moment. However, the comparison of measured peak intensity ratios with those expected from angular-momentum coupling meant that tentative spin assignments were possible. The low resolution available, along with $J = 1/2$ for the $7s^2S_{1/2}$ state, meant that the normal relation for the hyperfine transition intensities, $S_{FF'}$, between states of F and F' (with angular momentum J and J' , respectively) could be simplified to

$$\frac{S_{FF'}}{S_{JJ'}} = \frac{I + 1}{I}, \quad (2)$$

where I represents the nuclear spin of the isotope. Fitting routines applied to the data shown in Fig. 1 suggested a ratio of 1.7(3) for the intensities of the two structures. In conjunction with Eq. (2), this was consistent with a low-spin assignment. In order to assess the ratio of ground and isomeric states within the beam and their contribution to the structure of Fig. 1, additional decay spectroscopy measurements were performed.

A systematic error of 30 MHz was established for $A(7s^2S_{1/2})$ based on the scatter observed in the measured A factors of the ^{221}Fr reference scans [11,30]; however, this

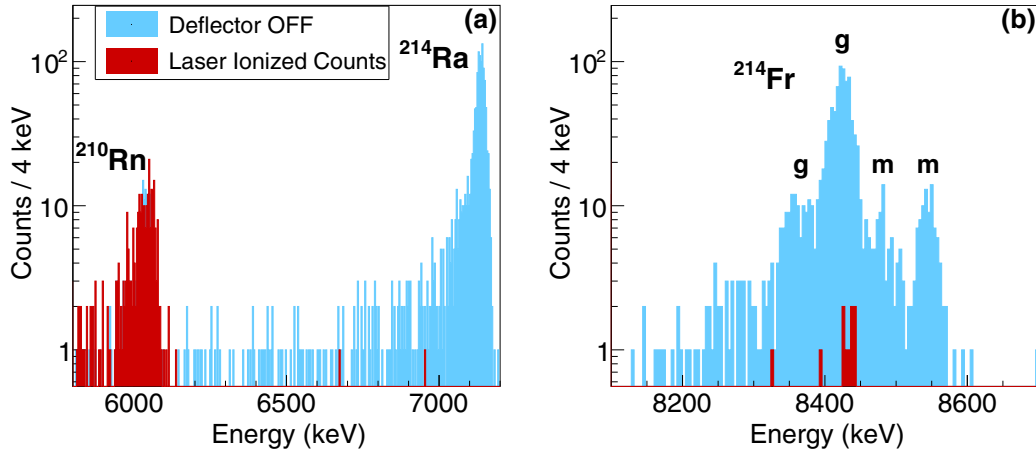


FIG. 2. α -decay energy spectra showing the content of the full (blue) and laser-ionized (red) ^{214}Fr beams at the DSS. (a) An α -decay energy spectrum for ^{214}Ra ($E_\alpha = 7137(3)$ keV, $t_{1/2} = 2.46(3)$ seconds [38]) and its daughter ^{210}Rn ($E_\alpha = 6041(3)$ keV, $t_{1/2} = 2.4(1)$ h [39]). (b) An α -decay energy spectrum for ^{214g}Fr and ^{214m}Fr ; lifetimes and decay energies can be found in Fig. 3.

uncertainty was mainly dominated by the limited resolution of the laser system. For the isotope shift, a minimum instrument error of 150 MHz was set. This accounted for the drift and fluctuations of the centroid frequency of ^{221}Fr , and the precision of the HighFinesse/Ångstrom WS7 wavelength meter. When the calculated weighted standard deviation of the isotope shift or $A(7s^2S_{1/2})$ parameter was greater than the minimum errors, these were quoted instead.

B. Decay spectroscopy of ^{214}Fr

Laser-assisted nuclear decay spectroscopy was performed for the ^{214}Fr ion beam in order to determine its ground and isomeric state content. Figures 2(a) and 2(b) show the α -decay spectra from the implantation of the full $A = 214$ beam, as well as the purified laser-ionized beam of ^{214}Fr into the carbon foils, for a collection time of 30 min. Relative to the centroid frequency of ^{221}Fr , the Ti:Sa laser frequency was detuned to 18.3 and 22.1 GHz, respectively, for each hyperfine structure observed in Fig. 1. The laser-ionized spectrum in Fig. 2(b) represents the sum of the two separate spectra obtained from this method. A selectivity of 3.3 [20] meant that the content of each peak could be analyzed separately at the DSS. The presence of ^{214}Ra as an isobaric contaminant was reduced from the laser-ionized spectrum by beam gating (see Sec. II). However, the impinging of its daughter isotope ^{210}Rn ($t_{1/2} = 2.4(1)$ h [39]) with the surface of the silicon detectors occurred whenever full ^{214}Fr beams were examined. This meant that its decay could still be seen when analyzing the laser-ionized beam, allowing the ^{210}Rn peak to be used for calibrating the energy scale for both spectra.

All expected α decays from Fig. 3 were observed for both ^{214g}Fr and ^{214m}Fr when the ion deflector after the CEC was switched off, with a ratio of approximately 8:1. However, the implantation of the laser-ionized beam resulted in lower statistics and a nonoptimal energy resolution for the silicon detectors, due to the influence of the laser light on the baseline of the detector signal. In addition, data taking for this measurement was stopped before it could be completed

(as this was performed at the end of the experiment), resulting in only a partial data set being obtained. Nonetheless, 10 counts were observed that corresponded to the decay of ^{214g}Fr , and none were seen for ^{214m}Fr . Given the observed $^{214g}\text{Fr} : ^{214m}\text{Fr}$ ratio of 8:1 with the full beam, a statistical analysis concluded there was a 100% confidence that the ground state was present in the laser-ionized beam. Additionally, there was an 82.5% confidence that no isomeric state was present in the laser-ionized beam. Although the possibility of a ground/isomeric state mix could not be ignored *a priori*, any existence of an

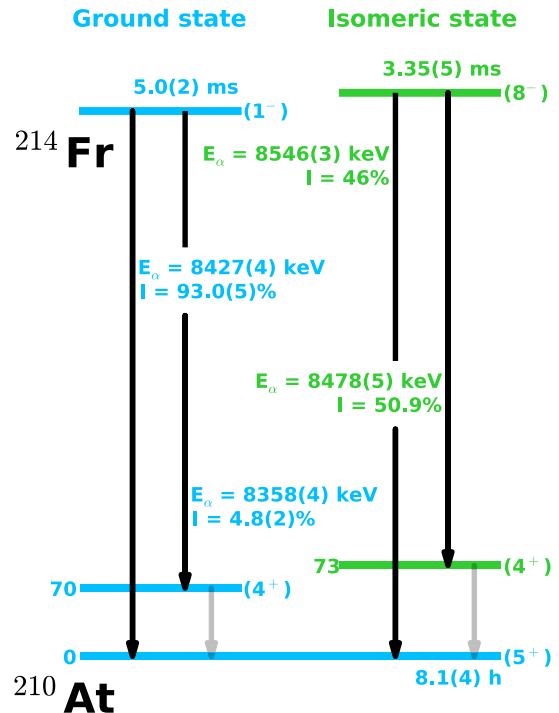


FIG. 3. The radioactive decay scheme of $^{214g,m}\text{Fr}$. The solid arrows represent the main α -decay paths [38] and the shaded arrows depict the allowed γ -ray transitions between given states.

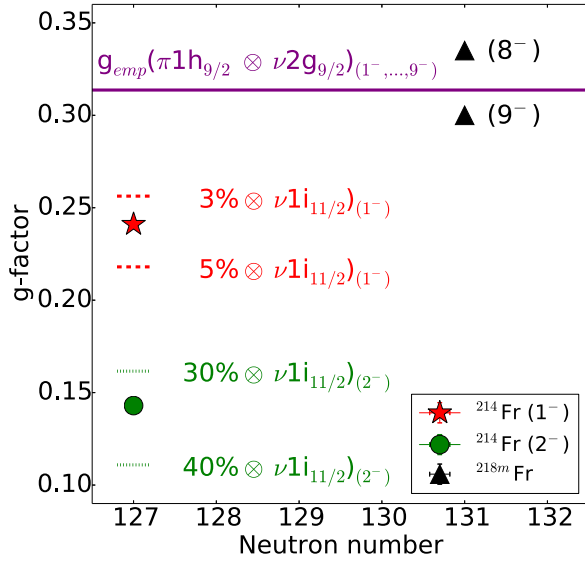


FIG. 4. Extracted ^{214g}Fr g factors for (1^-) and (2^-) spin assignments, alongside those for the tentative assignments of ^{218m}Fr [11]. Associated error bars are smaller than the data points. The g factors for a pure $(\pi 1h_{9/2} \otimes \nu 2g_{9/2})_{1^-}$ configuration and those with $(\pi 1h_{9/2} \otimes \nu 1i_{11/2})_{1^-}$ configuration mixing have been calculated empirically. See text for details.

isomeric state in Fig. 1 would have been suppressed by a factor of eight with respect to the ground state. This was consistent with background, meaning the isomeric state contribution could be neglected.

IV. DISCUSSION

To first order, odd-odd ^{214g}Fr involves the coupling of an unpaired valence proton located in the $\pi 1h_{9/2}$ orbital with a single valence neutron above the $N = 126$ shell gap, where $\nu 2g_{9/2}$ is the next spherical shell model orbital. This leads to possible ground state spin assignments of $(0, 1, 2, \dots)^-$, considering the lowest spin states from this multiplet. The observed hyperfine structure of the ground state in Fig. 1 automatically rules out a $I = (0^-)$ spin assignment, due to the observation of two peaks. Therefore, the use of $I = (1^-)$ and $I = (2^-)$ low-spin assignments were considered for the laser spectroscopy analysis following the observations presented above. Earlier α -decay spectroscopy studies have also ruled out the (0^-) spin assignment and suggest a (1^-) spin/parity, based on analogy with the isotope ^{210}Bi [44–46]. The extracted g -factor values for the (1^-) and (2^-) spin assignments are presented in Table I and shown graphically in Fig. 4. The

TABLE I. The $A(7s^2S_{1/2})$ factors, isotope shifts, g factors, and the change in the mean-square charge-radii for ^{214}Fr with respect to ^{221}Fr , for assumed (1^-) and (2^-) spin assignments. The statistical and systematic uncertainties for $\delta\langle r^2 \rangle^{221,214}$ are separated, enclosed within parentheses and brackets, respectively.

I^π	$A(7s^2S_{1/2})$ (GHz)	$\delta\nu^{221,214}$ (GHz)	g factor	$\delta\langle r^2 \rangle^{221,214}$ (fm ²)
(1^-)	+2.37(15)	+19.51(18)	+0.241(16)	-0.949(9){10}
(2^-)	+1.42(9)	+19.77(18)	+0.144(10)	-0.962(9){10}

calculation of the expected empirical g factor (represented by the purple solid line in Fig. 4) can be obtained from the additivity relation [47]. For the case where the proton and neutron spins are the same, the g factor of the weakly coupled pn configuration is independent of the spin to which they couple to. Individual empirical g factors for $\pi 1h_{9/2}$ and $\nu 2g_{9/2}$ were taken from the magnetic moments of the closest odd- A isotopes available: ^{213}Fr [35] and ^{211}Po [48], respectively.

Additionally, the $\nu 1i_{11/2}$ and $\nu 2g_{7/2}$ orbitals are also in the near vicinity [15] and their contributions to the total g factor due to configuration mixing with the $\nu 2g_{9/2}$ orbital need to be considered. With respect to the $\nu 1i_{11/2}$ orbital, only linear contributions are expected and this is reflected in Fig. 4. The experimental $g(^{214g}\text{Fr}_{I=(1^-)}) = +0.241(16)$ is consistent with a relatively pure $(\pi 1h_{9/2} \otimes \nu 2g_{9/2})_{1^-}$ configuration. It also compares to the g factors obtained for the tentative $I = (8^-)$ or $I = (9^-)$ assignments of ^{218m}Fr at $N = 131$, which is suggested to have a similar single-particle configuration with the protons and neutrons aligned [11]. The contribution due to configuration mixing with the $\nu 1i_{11/2}$ orbital (using the calculated magnetic moment for ^{209}Pb [49]) is relatively small, at 3.8%. However, in contrast, $\nu 1i_{11/2}$ configuration mixing accounts for 33.5% of the ^{214}Fr ground state assignment when $I = (2^-)$, with $g(^{214g}\text{Fr}_{I=(2^-)}) = +0.144(10)$. In either case, evidence of a contribution from the $\nu 1i_{11/2}$ orbital supports previous theoretical studies that require this in order to reproduce the kink in the mean square charge-radii values at the $N = 126$ shell closure [14,15,17]. For the $\nu 2g_{7/2}$ orbital, mixing calculations have been performed using the same empirical values as mentioned above for the $\pi 1h_{9/2}$, $\nu 2g_{9/2}$, and $\nu 2g_{7/2}$ orbitals, as well as the calculated $B(M1)$ value connecting the $\nu 2g_{9/2}$ and $\nu 2g_{7/2}$ orbitals [49]. These have shown that a 3.8% admixture of this type is sufficient to describe the measured g factor for ^{214}Fr in the case of $I = (1^-)$. For the $I = (2^-)$ assignment, however, the $\nu 2g_{7/2}$ orbital cannot contribute to the total g factor. Further study is required to confirm the ground-state spin and to investigate any possible shell effects that might be present, which will serve to test the robustness of the $N = 126$ shell closure.

The change in the mean-square charge-radii is interpreted in Fig. 5. Comparing the difference in the mean-square charge-radii before and after $N = 126$ offers an alternative way of isolating the effect seen at $N = 126$. This difference can be calculated by using

$$\delta\langle r^2 \rangle^{N,N'} = \delta\langle r^2 \rangle^{N,M} + \delta\langle r^2 \rangle^{M,N'}, \quad (3)$$

with N , N' representing the neutron numbers 125, 126 and 126, 127, for the differences before and after the shell closure respectively. The values for Hg-Ra are given in Table II and

TABLE II. Mean square charge-radii values just before and after the $N = 126$ shell closure for Hg to Ra, using Eq. (3) and literature mean square charge-radii values. The Fr $\delta \langle r^2 \rangle^{126,127}$ value corresponds to a (1^-) assignment and entries are marked with a ‘-’ where data is currently unavailable. Only statistical uncertainties are quoted for these values.

	Hg	Tl	Pb	Bi	Po	At	Rn	Fr	Ra
$\delta \langle r^2 \rangle^{125,126}$ (fm ²)	0.0654(25)	–	0.0720(1)	0.0710(22)	0.0813(12)	–	0.0735(1)	0.0790(1)	0.0773(39)
$\delta \langle r^2 \rangle^{126,127}$ (fm ²)	–	0.0782(130)	0.0910(5)	0.0990(34)	0.1040(12)	–	–	0.1056(92)	–
Refs.	[42]	[5]	[6]	[7]	[18]	–	[9]	This work, [10]	[43]

neutron numbers are used in the mean-square charge-radii superscripts to highlight the crossing of the $N = 126$ shell closure.

A first observation is that the gradient in the charge radii between the $N = 125$ and $N = 126$ isotones is smaller than the gradient between $N = 126$ and $N = 127$. The latter leads to the well-known kink in the radii values [4]. A second observation is that the change in the radii below $N = 126$ is more or less constant for all isotopes from Hg ($Z = 80$) up to Ra ($Z = 88$), while an increase of the slope in the kink is observed with an increasing number of protons beyond $Z = 82$. It should be noted that for the cases of ${}_{83}\text{Bi}$ and ${}_{84}\text{Po}$, large systematic uncertainties on the atomic parameters could affect this interpretation [50]. However, in accordance with Eq. (1) these uncertainties scale with the mass difference. Therefore, the close proximity of the charge-radii values in Fig. 5 with their references minimizes these systematic effects. Despite this, the francium data points for both spin assignments lie far away from this trend. Further studies on ${}^{214}\text{Fr}$ in higher resolution is needed to confirm this result and draw conclusions about the influence of the valence protons outside $Z = 82$ on the slope of the kink. Additionally, data from the ${}_{80}\text{Hg}$, ${}_{85}\text{At}$, ${}_{86}\text{Rn}$, and ${}_{88}\text{Ra}$ isotones are needed in order to fully establish the systematics in this region.

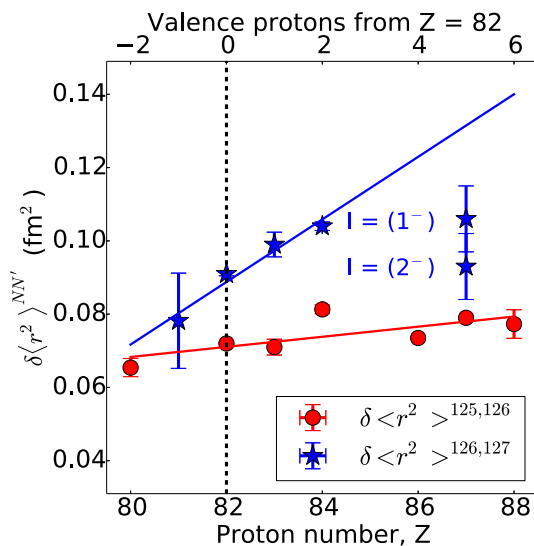


FIG. 5. The difference in the mean-square charge radii for before (red circles) and after (blue stars) the $N = 126$ shell closure, across the $N = 125$ and $N = 127$ isotone chains, using the values in Table II. The shell closure at $Z = 82$ is highlighted with a dashed line.

The question of how this mechanism arises is still debated. Modifications to the spin-orbit interaction in mean-field calculations have successfully reproduced the kink in the Pb and Po isotope chains [14,15,17]. Other studies suggest the inclusion of a density-dependent term to the spin-orbit term [13,16], with the latter also proposing the inclusion of three-nucleon ($3N$) interactions in mean-field calculations. However, mean-field theory is primarily limited to even-even nuclei. Such calculations are difficult to perform for nuclei with odd numbers of protons and neutrons such as ${}_{87}^{214}\text{Fr}_{127}$, and this poses a major challenge for theoretical nuclear physics [51]. Recently, modified mean-field methods have allowed calculations to extend to odd- A nuclei, giving reasonable descriptions to light-mass nuclei such as ${}^{25}\text{Mg}$ [52]. Density functional theory (DFT) has also been developed in recent years and it is hoped that this can be applied across the entire nuclear landscape [53]. At present, a limited framework exists for mean-field calculations in this area of the nuclear chart and the mechanism remains an open question. Further studies are required to expand on the current nuclear theory constraints and it is anticipated that future developments of DFT calculations can be extended to include calculations for heavy-mass nuclei. Experimentally, the study of other $N = 127$ isotones is desirable in order to further assert whether a dependence exists between the magnitude of these kinks and the proton number.

V. CONCLUSION

The neutron-deficient isotope ${}^{214}\text{Fr}$ has been studied at the CRIS beam-line at ISOLDE. With a half-life of 5.0(2) ms, ${}^{214g}\text{Fr}$ represents the shortest-lived isotope studied online with laser spectroscopic techniques. A comparison between empirical and experimentally obtained g factors suggest that whilst the possible $I = (1^-)$ assignment is dominated by a $(\pi 1h_{9/2} \otimes \nu 2g_{9/2})$ configuration, the alternative $I = (2^-)$ assignment involves more configuration mixing with the $\nu 1i_{11/2}$ orbital. Further investigation into possible shell effects involving this orbital is required for a definitive assignment. The charge-radii value past the $N = 126$ shell closure shows the expected kink and is comparable to the behavior exhibited in the neighboring isotones.

ACKNOWLEDGMENTS

We acknowledge the support of the ISOLDE collaboration and technical teams, and the GSI target laboratory for producing the carbon foils. This work was supported by the

IUAP-Belgian State Belgian Science Policy (BRIX network P7/12), FWO-Vlaanderen (Belgium), and GOA 015/10 from KU Leuven; ERC Consolidator Grant No. 648381; the Science and Technology Facilities Council Consolidated Grant No. ST/F012071/1, Continuation Grant No. ST/J000159/1, and Ernest Rutherford Grant No. ST/L002868/1; and the European Union's Seventh Framework Programme for Research and Technological Development under Grant

Agreements No. 262010 (ENSAR), No. 267194 (COFUND), and No. 289191 (LA³NET). T.E.C. was supported by the STFC Ernest Rutherford Fellowship No. ST/J004189/1. K.T.F. was supported by STFC Advanced Fellowship Scheme Grant No. ST/G006415/1. K.M.L. was supported by the FWO Pegasus Marie Curie Fellowship under Grant No. 267216. We acknowledge the financial aid from the Ed Schneiderman Fund at New York University.

- [1] P. G. Hansen *et al.*, *Phys. Lett. B* **28**, 415 (1969).
 [2] A. N. Andreyev *et al.*, *Nature* **405**, 430 (2000).
 [3] L. P. Gaffney *et al.*, *Nature* **497**, 199 (2013).
 [4] P. Campbell, I. D. Moore, and M. R. Pearson, *Prog. Part. Nucl. Phys.* **86**, 127 (2016).
 [5] A. E. Barzakh, L. K. Batist, D. V. Fedorov, V. S. Ivanov, K. A. Mezilev, P. L. Molkanov, F. V. Moroz, S. Y. Orlov, V. N. Panteleev, and Y. M. Volkov, *Phys. Rev. C* **88**, 024315 (2013).
 [6] R. C. Thompson *et al.*, *J. Phys. G* **9**, 443 (1983).
 [7] M. R. Pearson, P. Campbell, K. Leerunnavarat *et al.*, *J. Phys. G* **26**, 1829 (2000).
 [8] T. E. Cocolios, W. Dexters, M. D. Seliverstov, A. N. Andreyev, S. Antalic, A. E. Barzakh, B. Bastin, J. Büscher, I. G. Darby, D. V. Fedorov, V. N. Fedosseev, K. T. Flanagan, S. Franchoo, S. Fritzsche, G. Huber, M. Huyse, M. Keupers, U. Köster, Y. Kudryavtsev, E. Mané, B. A. Marsh, P. L. Molkanov, R. D. Page, A. M. Sjoedin, I. Stefan, J. Van de Walle, P. Van Duppen, M. Venhart, S. G. Zemlyanoy, M. Bender, and P. H. Heenen, *Phys. Rev. Lett.* **106**, 052503 (2011).
 [9] W. Borchers *et al.*, *Hyperfine Interact.* **34**, 25 (1987).
 [10] V. A. Dzuba, W. R. Johnson, and M. S. Safronova, *Phys. Rev. A* **72**, 022503 (2005).
 [11] I. Budinčević, J. Billowes, M. L. Bissell, T. E. Cocolios, R. P. de Groote, S. De Schepper, V. N. Fedosseev, K. T. Flanagan, S. Franchoo, R. F. Garcia Ruiz, H. Heylen, K. M. Lynch, B. A. Marsh, G. Neyens, T. J. Procter, R. E. Rossel, S. Rothe, I. Strashnov, H. H. Stroke, and K. D. A. Wendt, *Phys. Rev. C* **90**, 014317 (2014).
 [12] S. A. Ahmad *et al.*, *Phys. Lett. B* **133**, 47 (1983).
 [13] M. M. Sharma, G. Lalazissis, J. König, and P. Ring, *Phys. Rev. Lett.* **74**, 3744 (1995).
 [14] P. G. Reinhard and H. Flocard, *Nucl. Phys. A* **584**, 467 (1995).
 [15] P. M. Goddard, P. D. Stevenson, and A. Rios, *Phys. Rev. Lett.* **110**, 032503 (2013).
 [16] H. Nakada and T. Inakura, *Phys. Rev. C* **91**, 021302(R) (2015).
 [17] J. P. Ebran, A. Mutschler, E. Khan, and D. Vretenar, *Phys. Rev. C* **94**, 024304 (2016).
 [18] M. D. Seliverstov, T. E. Cocolios, W. Dexters *et al.*, *Phys. Lett. B* **719**, 362 (2013).
 [19] K. T. Flanagan, K. M. Lynch, J. Billowes, M. L. Bissell, I. Budinčević, T. E. Cocolios, R. P. de Groote, S. De Schepper, V. N. Fedosseev, S. Franchoo, R. F. Garcia Ruiz, H. Heylen, B. A. Marsh, G. Neyens, T. J. Procter, R. E. Rossel, S. Rothe, I. Strashnov, H. H. Stroke, and K. D. A. Wendt, *Phys. Rev. Lett.* **111**, 212501 (2013).
 [20] K. M. Lynch, J. Billowes, M. L. Bissell, I. Budinčević, T. E. Cocolios, R. P. De Groote, S. De Schepper, V. N. Fedosseev, K. T. Flanagan, S. Franchoo, R. F. Garcia Ruiz, H. Heylen, B. A. Marsh, G. Neyens, T. J. Procter, R. E. Rossel, S. Rothe, I. Strashnov, H. H. Stroke, and K. D. A. Wendt, *Phys. Rev. X* **4**, 011055 (2014).
 [21] R. P. de Groote, I. Budinčević, J. Billowes, M. L. Bissell, T. E. Cocolios, G. J. Farooq-Smith, V. N. Fedosseev, K. T. Flanagan, S. Franchoo, R. F. Garcia Ruiz, H. Heylen, R. Li, K. M. Lynch, B. A. Marsh, G. Neyens, R. E. Rossel, S. Rothe, H. H. Stroke, K. D. A. Wendt, S. G. Wilkins, and X. Yang, *Phys. Rev. Lett.* **115**, 132501 (2015).
 [22] K. M. Lynch, T. E. Cocolios, J. Billowes, M. L. Bissell, I. Budinčević, T. Day Goodacre, R. P. de Groote, E. J. Farooq-Smith, V. N. Fedosseev, K. T. Flanagan, S. Franchoo, R. F. Garcia Ruiz, H. Heylen, R. Li, B. A. Marsh, G. Neyens, R. E. Rossel, S. Rothe, H. H. Stroke, K. D. A. Wendt, S. G. Wilkins, and X. Yang, *Phys. Rev. C* **93**, 014319 (2016).
 [23] M. M. Rajabali, K. M. Lynch, T. E. Cocolios *et al.*, *Nucl. Instrum. Methods A* **707**, 35 (2013).
 [24] S. C. Wu, *Nucl. Data Sheets* **110**, 681 (2009).
 [25] E. Kugler, *Hyperfine Interact.* **129**, 23 (2000).
 [26] A. Herlert, *Nucl. Phys. News* **20**, 5 (2010).
 [27] J. Lettry *et al.*, *Nucl. Instrum. Methods B* **126**, 130 (1997).
 [28] H. Frånberg *et al.*, *Nucl. Instrum. Methods B* **266**, 4502 (2008).
 [29] E. Mané *et al.*, *Eur. Phys. J. A* **42**, 503 (2009).
 [30] T. E. Cocolios *et al.*, *Nucl. Instrum. Methods B* **317**, 565 (2013).
 [31] T. E. Cocolios, R. P. de Groote *et al.*, *Nucl. Instrum. Methods B* **376**, 284 (2016).
 [32] S. Rothe *et al.*, *Nucl. Instrum. Methods B* **317**, 561 (2013).
 [33] B. A. Marsh *et al.*, *Nucl. Instrum. Methods B* **317**, 550 (2013).
 [34] R. E. Rossel *et al.*, *Nucl. Instrum. Methods B* **317**, 557 (2013).
 [35] A. Coc *et al.*, *Phys. Lett. B* **163**, 66 (1985).
 [36] C. Ekström *et al.*, *Hyperfine Interact.* **4**, 165 (1978).
 [37] E. Gomez, S. Aubin, L. A. Orozco, G. D. Sprouse, E. Iskrenova-Tchoukova, and M. S. Safronova, *Phys. Rev. Lett.* **100**, 172502 (2008).
 [38] M. S. Basunia, *Nucl. Data Sheets* **121**, 561 (2014).
 [39] F. G. Kondev, *Nucl. Data Sheets* **109**, 1527 (2008).
 [40] J. S. Grossman, L. A. Orozco, M. R. Pearson, J. E. Simsarian, G. D. Sprouse, and W. Z. Zhao, *Phys. Rev. Lett.* **83**, 935 (1999).
 [41] J. Zhang, M. Tandecki, R. Collister, S. Aubin, J. A. Behr, E. Gomez, G. Gwinner, L. A. Orozco, M. R. Pearson, and G. D. Sprouse, *Phys. Rev. Lett.* **115**, 042501 (2015).
 [42] G. Ulm *et al.*, *Z. Phys. A* **325**, 247 (1986).
 [43] L. W. Wansbeek, S. Schlessler, B. K. Sahoo, A. E. L. Dieperink, C. J. G. Onderwater, and R. G. E. Timmermans, *Phys. Rev. C* **86**, 015503 (2012).
 [44] D. F. Torgerson, R. A. Gough, and R. D. Macfarlane, *Phys. Rev.* **174**, 1494 (1968).
 [45] K. Valli and E. K. Hyde, *Phys. Rev.* **176**, 1377 (1968).

- [46] D. F. Torgerson and R. D. Macfarlane, *Phys. Rev. C* **2**, 2309 (1970).
- [47] G. Neyens, *Rep. Prog. Phys.* **66**, 633 (2003).
- [48] M. D. Seliverstov, T. E. Cocolios, W. Dexters, A. N. Andreyev, S. Antalic, A. E. Barzakh, B. Bastin, J. Büscher, I. G. Darby, D. V. Fedorov, V. N. Fedosseev, K. T. Flanagan, S. Franchoo, G. Huber, M. Huyse, M. Keupers, U. Köster, Y. Kudryavtsev, B. A. Marsh, P. L. Molkanov, R. D. Page, A. M. Sjödin, I. Stefan, P. Van Duppen, M. Venhart, and S. G. Zemlyanoy, *Phys. Rev. C* **89**, 034323 (2014).
- [49] R. Bauer, J. Speth *et al.*, *Nucl. Phys. A* **209**, 535 (1973).
- [50] B. Cheal, T. E. Cocolios, and S. Fritzsche, *Phys. Rev. A* **86**, 042501 (2012).
- [51] F. Chappert, N. Pillet, M. Girod, and J. F. Berger, *Phys. Rev. C* **91**, 034312 (2015).
- [52] B. Bally, B. Avez, M. Bender, and P. H. Heenen, *Phys. Rev. Lett.* **113**, 162501 (2014).
- [53] J. Dobaczewski, M. V. Stoitsov, W. Nazarewicz, and P. G. Reinhard, *Phys. Rev. C* **76**, 054315 (2007).